Int J Adv Manuf Technol (2016) 86:3383–3394
DOI 10.1007/s00170-016-8452-4

ORIGINAL ARTICLE

Effect of hybrid texture combining micro-pits and micro-grooves on cutting performance of WC/Co-based tools

Jialin Sun[1] · **Yonghui Zhou**[1] · **Jianxin Deng**[1] · **Jun Zhao**[1]

Received: 24 November 2015 / Accepted: 1 February 2016 / Published online: 13 February 2016

Abstract Friction at the tool-chip interface may be reduced by introducing a lubricant into the tool-chip interface; the effectiveness of which can be enhanced by surface texturing the tool. Micro-grooves, micro-pits, and hybrid texture combining micro-pits and micro-grooves were fabricated employing laser on the rake face of carbide tools, with a view to facilitating lubricant penetrate and retention; then, solid lubricant (molybdenum disulfide) was applied to fill micro-textures to form micro-pools. In the present study, the effect of hybrid texture on the cutting performance was experimentally investigated using the hybrid-textured tools, single-textured tools, and conventional tools in dry turning pure iron tests on the numerical control lathe. The behavior of these tools was quantified in terms of the cutting forces, cutting temperature, friction coefficient at the tool-chip interface, shear angle, surface roughness of machined workpiece, chip morphology, and tool wear on the rake face. Results confirm enhanced cutting performance of hybrid-textured tools by collaborative complementation as micro-reservoir for constant lubricant replenishment of micro-grooves and micro-pits. It is suggested that the hybrid-textured self-lubricating tool is applicable to a stable dry cutting of pure iron.

Keywords Micro-pits · Micro-grooves · Hybrid textures · Pure iron · Cutting performance

✉ Jianxin Deng
jxdeng@sdu.edu.cn

[1] Key Laboratory of High Efficiency and Clean Mechanical Manufacture of MOE, Department of Mechanical Engineering, Shandong University, No. 17923 Jingshi Road, 250061 Jinan, Shandong Province, People's Republic of China

1 Introduction

As a very special ferrous metal featuring excellent toughness, plasticity, and electromagnetism, pure iron has gradually become the material basis of many high-tech industries [1]. But, its application was limited by high machining cost owing to its poor machinability. This is because the progressive friction at tool-chip interface accelerates the tool wear, especially adhesive wear.

Recently, the dry cutting of pure iron without any coolant has been given increasing attention. Xu et al. [2] performed experiments on pure iron using a cemented carbide-coated blade and showed that the high plasticity of pure iron caused an increased difficulty chip breaking and thus produced an intimate contact between the chip and the rake face, which prevented coolant entering into the tool-chip interface. Using a coated tool does not always improve tool cutting performance in turning pure iron. As Kong et al. [3] summarized, the main wear mechanism of cutting pure iron was adhesive wear and TiAlN coatings cannot effectively increase the tool adhesive wear resistance. These researches have not yet significantly improved dry machining performance of pure iron owing to a severe tool-chip adhesion existing in dry cutting.

Micro-structured rake face can effectively improve the surface tribological characteristics and decrease the tool-chip friction coefficient [4–9]. Sugihava and Enomoto [10] suggested that the developed micro-grooved tools with micro-grooves appropriate deep had an excellent anti-adhesive property in dry cutting. Functional structured surface could change the chip compression factor and normal force [11].

Another development in increasing tool wear resistance in machining is by means of internal lubrication. Micro-textures filled with lubricant can extremely contribute to reducing friction and wear for sliding contact [12–14]. Under high pressure and temperature, the lubricant trapped in the micro-textures

between the chip and tool can be squeezed into the interface to improve tribological properties. Furthermore, solid lubricant with layered structure can form a solid lubricating film at the tool-chip interface resulting in friction occurring within the film [15–18].

As well known, micro-texture fabricated on the tool rake face using laser and filled with lubricant can act as micro-pools and thus reducing friction and wear at the tool-chip interface. However, current studies mainly focus on the shape of single texture on the performance acting as micro-pool, neglecting hybrid texture combining single textures of different shapes. Hybrid-textured micro-pool lubricated tool may well outperform single-textured micro-pool lubricated tool. In an earlier study by Suh et al. [19], he proposed multi-scale textures of circles and ellipses and suggested that the multi-scale-textured surface had lower friction coefficient performance than the single-textured surface due to hydrodynamic lubrication effect. Ruan and Lu [20] researched the hydrodynamic lubrication performance on multi-textured surface structured by multi-arcs and triangle texture; it was found that the multi-textured surface performed better in comparison with the independent-textured surface. The former gives a more appropriate pressure distribution and thus produces a higher thrust force. Yin et al. [21] created composite textures on cylinder liner and summarized that the lubrication performances of composite textures were obviously superior to that of single textures, and the effective area was extended by collaborative complementation of micro-grooves and micro-dimples to increasing lubricating film pressure.

This paper focuses on cutting tool lubrication and investigates the use of internal micro-pool lubrication of hybrid textures combining micro-pit lubrication and micro-groove lubrication for a cutting tool.

2 Experiment details

2.1 The cutting mechanism of pure iron

The iron materials with carbon content less than 0.0218 % are called pure iron. The metallographic micro-structure is mainly ferrite at room temperature. The chemical compositions of pure iron are shown in Table 1. The physical and mechanical property comparison of pure iron and American Iron and Steel Institute (AISI) 1045 steel are listed in Table 2. The hardness of pure iron is HBW100 lower than that of normalized AISI 1045 steel. The strength of pure iron is 313.6 MPa lower than that of normalized AISI 1045 steel. The thermal conductivity and elastic modulus are close to those of normalized AISI 1045 steel, whereas the elongation of pure iron is 3.1 times of AISI 1045 steel and the impact value is 6 times that of AISI 1045 steel [22, 23]. Therefore, features in machining pure iron material are listed as follows: rapidly severe tool wear by reason of higher chip plastic deformation and grievous work hardening, chip easily adhered on the rake face of cutting tool; poor machining surface quality owing to that the chip is hard curled and broken and for the most part winded on workpiece and rake face of cutting tool; and prone to forming built-up edge [24].

2.2 Fabrication of micro-textured self-lubricating tools

Tungsten carbide/cobalt (WC/Co) cemented carbide was selected as a cutting tool material for this study. Composition and physical and mechanical properties of this tool material are listed in Table 3. The dimensions of the turning tools were 16 × 16 × 5 mm. The rake face and flank face of these tools were finished by grinding and polishing to the roughness R_a of less than 0.02 μm and then were cleaned with a 30-min ultrasonic bath in alcohol and acetone, respectively. An Nd:YAG laser was used to machining different kinds of micro-textures including micro-grooves, micro-pits, and hybrid texture combining micro-grooves and micro-pits on the rake face. The parameters of these micro-textures are listed in Table 4. Buildup of material often occurs around the grooves and pits during the laser texturing process; thus, a deburring process was needed before the embedding. The rake face was ground lightly on the obscured glass until the laser burr was all removed and then was cleaned with a 20-min ultrasonic bath in alcohol and acetone, respectively, and dried for approximately 20 min in pre-vacuum dryer. Then, MoS_2 power was embedded into the micro-textures using self-designed tools whose shape was similar to a spoon under the tool microscope.

Figure 1 shows the three different kinds of micro-graphs of surface textures on the rake face of carbide insert. Figure 1d shows the micro-graphs of hybrid-textured self-lubricating tool. Figure 1e shows the cross-section micro-graph of micro-groove, and Fig. 1f shows the cross-section micro-graph of micro-pit.

2.3 Cutting tests

Turning tests were carried out on a numerical control lathe (CKD6150H, Dezhou PuLiSen Machine Tool Co. Ltd., China) equipped with a commercial tool holder having the

Table 1 Chemical composition of pure iron material

Element	Fe	C	Si	Mn	Ni	S	Cr	Cu	P	Al
Wt%	>99.8	0.013	0.028	0.029	0.035	0.02	0.02	0.034	0.0072	0.0023

Table 2 The physical and mechanical property comparison of pure iron and AISI 1045 steel

Material	Hardness (HB)	Tensile strength σ_b (kg f/mm^2)	Elongation δ (%)	Impact value α_k (k gf/cm^2)	Thermal conductivity λ (cal/cm · s)
AISI 1045 steel (normalizing)	<229	61	16	5	0.120
Pure iron	100	25	50	30	0.1~0.15

following geometry: rake angle $\gamma_0 = 10°$, clearance angle $\alpha_o = 10°$, inclination angle $\lambda_s = 1°$, and side cutting edge angle $K_r = 50°$. The workpiece material used was pure iron with a hardness of HRB100 in the form of a round bar with an external diameter of 100 mm. The turning tools used were micro-textured self-lubricating tools and the conventional tools whose rake face and flank face were finished by grinding and polishing to the roughness R_a of less than 0.02 μm but not machined micro-textures. All tests were performed in continuous dry cutting with the following parameters: cutting speed $v = 60$–120 m/min, depth of cut $a_p = 0.2$ mm, feed rate $f = 0.1$ mm/rev, and cutting time $t = 150$ s. The machining parameters were selected after some initial trials so that well-defined wear marks on the tool rake face were generated under such conditions.

Cutting forces were obtained with a KISTLER 9275A piezoelectric quartz dynamometer linked via charge amplifiers to chart recorder. Cutting temperatures were obtained with an infrared thermography (TH5104, NEC Group Co. Ltd., China). The machined surface roughness was measured by a roughmeter (TR200, HMCT Group Co. Ltd., China). The macro-morphology of chips was surveyed by an optical microscope (VHX-600E, KEYENCE Inc., Japan). The morphologies of worn region of the cutting tools were examined by scanning electron microscopy (SEM; QUANTAFEG 250, FEI Inc., USA), and the chemical composition at the wear track was identified by energy-dispersive X-ray spectroscopy (EDX; X-MAX30, Oxford Instruments Inc., UK).

3 Results and discussion

3.1 Cutting force

Figure 2 presents the graphs of the three cutting force components (main cutting force F_z, radial thrust force F_y, and axial thrust force F_x) at different cutting speeds with GT, PT, GPT, and CT tools. Each point of the curve represents the average cutting forces measured in the stable cutting process of four times repeated experiments, while the error bars represent the dispersion of the results. Cutting speeds seem to have an effect on the cutting forces of the tools. It is evident that the cutting forces were decreased slightly along with the increasing cutting speeds in the whole experimental range. The presence of micro-textures created by laser surface texturing technique significantly reduced the average cutting forces. The cutting behavior of the micro-textured self-lubricating tools and CT tools differed more evidently in high cutting speed. In case of high-speed cutting (120 m/min), compared to CT tool, the main cutting force F_z of GT was reduced by 3.1 %, the main cutting force F_z of PT was reduced by 10.5 %, and the main cutting force F_z of GPT was reduced by 15.4 %.

It indicated that the shape of the patterned micro-textures played a key role in the cutting performance of micro-textured self-lubricating tools. The hybrid-textured self-lubricating tools were found to yield the lowest cutting forces, followed by PT tools, and the GT tools were the highest. In case of high cutting speed (120 m/min), compared to GT tool, the axial thrust force F_x of GPT tool was reduced by 33.3 %, the radial thrust force F_y of GPT tool was reduced by 26.6 %, and the main cutting force F_z of GPT tool was reduced by 12.7 %. Compared to PT tool, the axial thrust force F_x of GPT tool was reduced by 18.5 %, the radial thrust force F_y of GPT tool was reduced by 13.4 %, and the main cutting force F_z of GPT tool was reduced by 7.1 %.

When the friction between flank face and transitional surface or machined surface is small, cutting forces and tool geometry angles approximately conform to the formula [25].

$$Fy/Fz = \tan(\beta - \gamma o) \tag{1}$$

According to this formula, we can easily get the calculating formula for average friction coefficient at the tool-chip interface.

$$\mu = \tan(\beta) = \tan(\gamma o + \arctan(Fy/Fz)) \tag{2}$$

Table 3 Properties of the cemented carbide materials

Composition (wt%)	Density (g/cm^3)	Hardness (GPa)	Flexural strength (MPa)	Fracture toughness (MPa m$^{1/2}$)	Thermal conductivity (W/mk)	Thermal expansion coefficient (10^{-6}/k)
WC + 6 % Co	14.6	16.0	2300	14.8	75.4	4.51

Table 4 The parameters of micro-textures

Texture types	Width or diameter (μm)	Depth (μm)	Period (μm)	The distance to cutting edge (μm)	Code
Micro-grooves	40	50	100	150	GT
Micro-pits	40	50	60,100	150	PT
Hybrid textures	40/40	50	60,100	150	GPT

Note that 100 is the two adjacent lines spacing and 60 is the center distance of two adjacent pits in the same line

where β is the friction angle, γ_o is the rake angle, F_y is the radial thrust force, and F_z is the main cutting force.

Figure 3 shows the average friction coefficients at the tool-chip interface of GT, PT, GPT, and CT tools at different

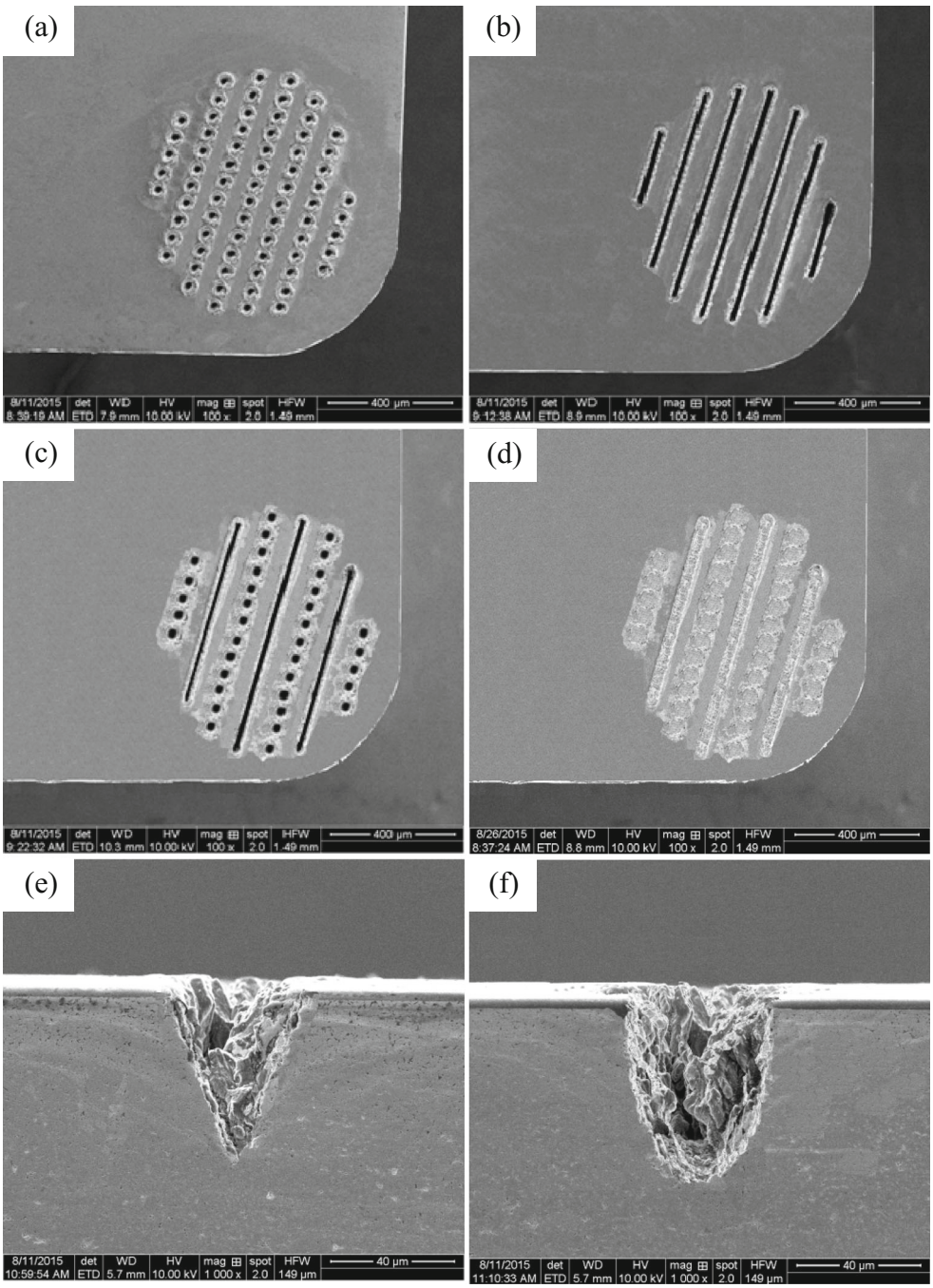

Fig. 1 Micro-graphs of surface textures on the rake face of carbide insert, **a** GT, **b** PT, **c** GPT, and **d** micro-graphs of GPT tool rake face filled with lubricant; cross-section micro-graph of micro-groove (**e**) and micro-pit (**f**)

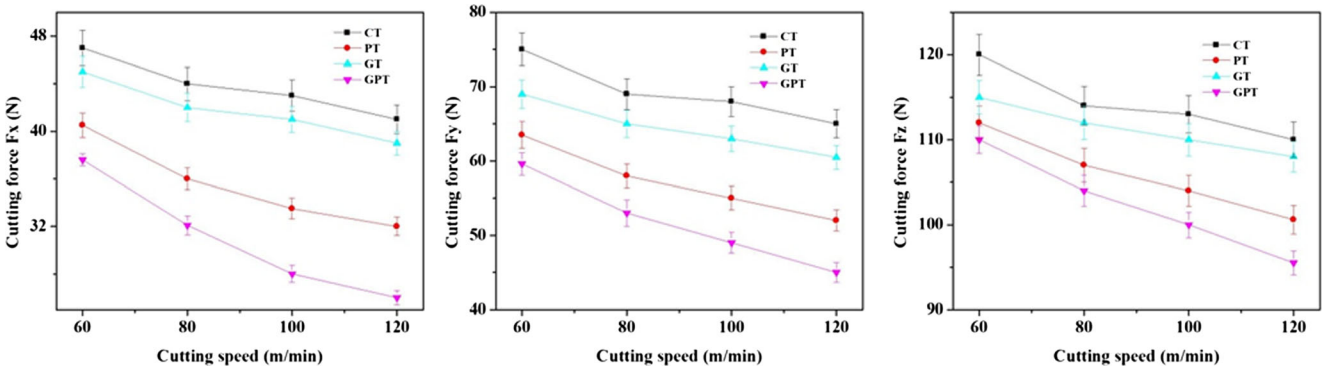

Fig. 2 Cutting forces of four different kinds of tools at different cutting speeds

cutting speeds. It turned out that the average friction coefficients at the tool-chip interface were decreased with increasing of cutting speeds. There was a clear decrease in average friction coefficient between micro-textured self-lubricating tools and CT tools. As was shown in the chart, we can conclude that the shape of micro-textures can be optimized to greatly reduce the average friction coefficient. Micro-pits showed better tribological performance than micro-grooves. Compared to single micro-texture, hybrid textures of micro-pits and micro-grooves can further improve the tribological performance. In case of high cutting speed (120 m/min), compared to GT tool, the tool-chip average friction coefficient with GPT tool was reduced by 14.5 %, and compared to PT tools, the tool-chip average friction coefficient with GPT tool was reduced by 8.5 %.

Shear angle is the angle between shear sliding plane and cutting speed. Shear angle can directly reflect cutting deformation. Moreover, it can affect the distributing of stress on rake face and the contact length between chip and rake face. Above all, it has a significant effect on the workpiece surface quality. Shear angle Φ can be calculated according the formula [26, 27]

$$\phi = \frac{\pi}{4} + \frac{\gamma o}{2} - \frac{\beta}{2} \tag{3}$$

where β is the friction angle and γ_o is the rake angle.

Based on Eqs. (1) and (3), the shear angle can be calculated easily. Figure 4 presents the graph of the shear angle at different cutting speeds with GT, PT, GPT, and CT tools. According to Figs. 3, 4, and 5, we can see that the smaller cutting force and friction coefficient can contribute to the increase of shear angle, which can decrease the deformation of chip, make the cutting process more stable, and then guarantee the cutting quality. Similarly, the shear angle of hybrid-textured self-lubricating tools was larger than that of single-textured self-lubricating tools. In case of high cutting speed (120 m/min), compared to GT tools, the shear angle of chip with GPT tools was increased by 5.5 %, and compared to PT tools, the shear angle of chip with GPT tools was increased by 3.4 %.

3.2 Cutting temperature

In this paper, the cutting temperatures were obtained with an infrared thermography (TH5104, NEC Group Co. Ltd., China). The measuring principle is, when heated, the cutting tool, chip, and workpiece will produce light and heat radiation with a certain intensity and the intensity would increase with cutting temperature. So, we can indirectly determine the cutting temperature by measuring the optical and thermal

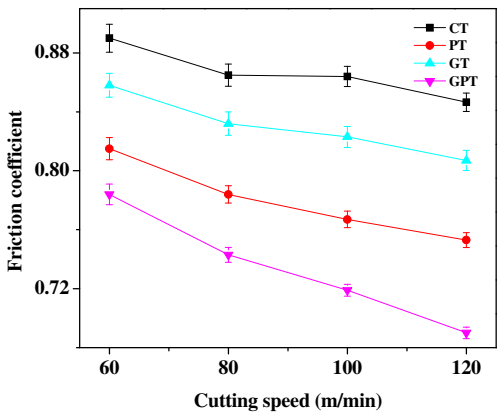

Fig. 3 Friction coefficient between the tool-chip interface of four kinds of tools at different cutting speeds

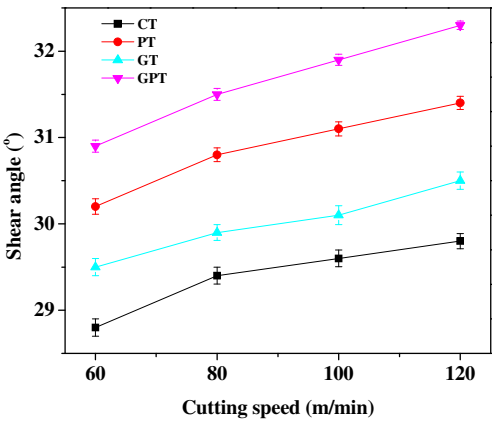

Fig. 4 Shear angle at different cutting speeds with GT, PT, GPT, and CT tools

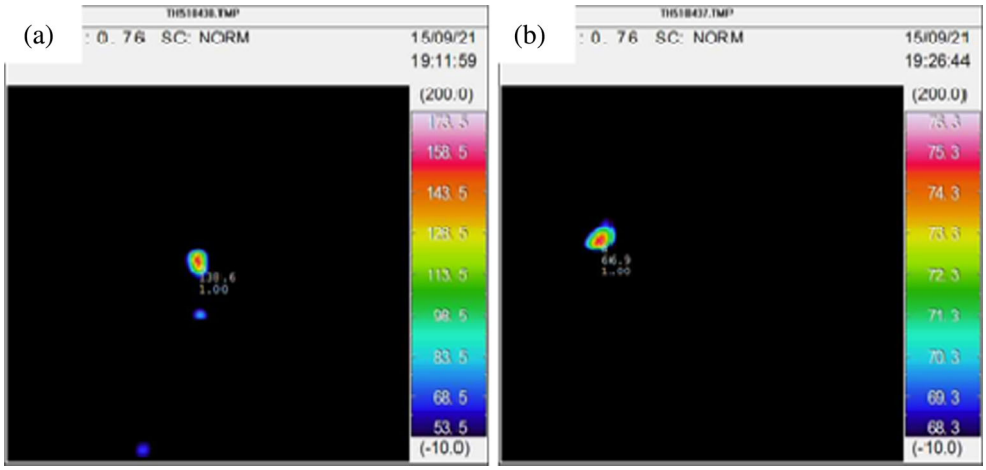

Fig. 5 The cutting temperature distribution diagrams with the CT tool (**a**) and GPT tool (**b**) at the cutting speed of 60 m/min

radiation. It has been proven that the highest cutting temperature of tool rake face is not located on cutting edge but on the area near the main cutting edge. Therefore, we choose to put the infrared thermal imaging instrument to the location which is close to the tool nose and main cutting edge on tool rake face. When the cutting continues to 60 s, we would take five pictures in a row. Figure 5 shows the cutting temperature distribution diagrams with the CT tool and GPT tool at the cutting speed of 60 m/min taken with TH5104 infrared thermal imaging instrument. Figure 6 demonstrated the cutting temperature of four kinds of tools at different speeds. Each point of the curve represents the average temperature of five highest temperatures obtained from five sequent temperature distribution photos. Therefore, in this paper, the cutting temperature can be the highest temperature of the tool rake face.

Figure 6 exhibited that there was a marked decrease in cutting temperature between micro-textured self-lubricating tools and CT tools in dry cutting. The cutting temperatures increased with the increasing of cutting speeds. The decreasing effectiveness was visible for all the cutting speeds, but difference between cutting temperature values caused by surface texturing was also larger for higher speeds. The graph led us to the conclusion that the shape of micro-texture was critical to decrease the cutting temperature. In other words, there was a difference in the performance in reducing heat among different kinds of micro-textures. In case of high-speed cutting (120 m/min), compared to GT tools, the cutting temperature with GPT tools was reduced by 21.7 %, and compared to PT tools, the cutting temperature of GPT tools was reduced by 6.9 %. This is, in the aspect of performance in reducing heat, hybrid textures showed a better performance than single textures.

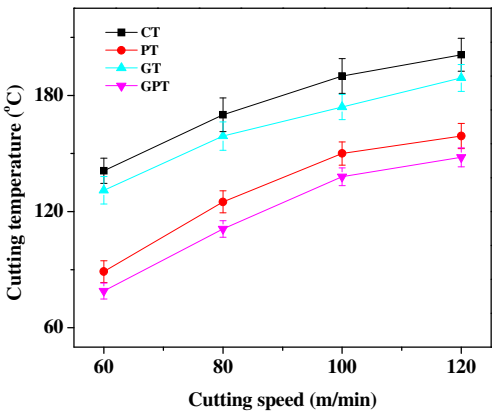

Fig. 6 Cutting temperature of four kinds of tools at different speeds

3.3 Surface roughness of machined workpiece

It is well known that surface roughness is often utilized to evaluate the cutting quality. The surface roughness to evaluate the surface quality of parts in machining is an important indicator; to some extent, it reflects the parts of surface machining quality. Figure 7 demonstrates the graph of the surface roughness R_a at different cutting speeds with GT, PT, GPT, and CT tools. The R_a was a mean value of 35 measured points at different positions, and the error bar was the surface roughness deviation of the measured 35 points. Following a 150-s cutting

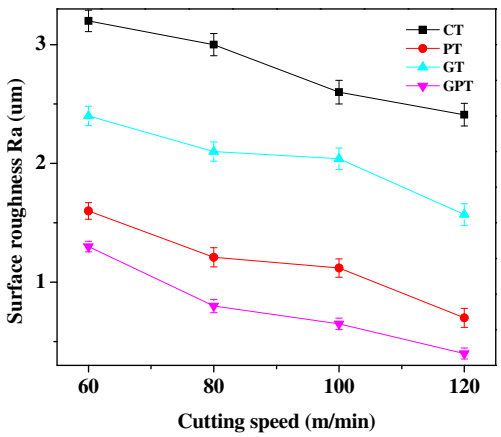

Fig. 7 Workpiece surface roughness R_a with different tools at different cutting speeds

process, it can be noticed that the micro-textured self-lubricating tools provided a better surface finish, and the surface roughness stability of machined workpiece during the experimental process was also increased by micro-textured self-lubricating tools. The micro-texture shape played an indispensable part on improving the machined surface quality. Compared with single-textured self-lubricating tools, hybrid-textured self-lubricating tools provided a better surface finish.

3.4 Discussion

In this paper, the authors developed three kinds of micro-scale-textured tools (micro-grooved tool, micro-pitted tool, and hybrid-textured tool) and studied their performance in cutting of pure iron under conditions of solid lubricating MoS_2. The results show that the cutting performance of hybrid-textured tool is obviously better than that of single-textured tool.

Figures 8, 9, and 10 illustrated micro-graphs of the wear track at the rake face and the corresponding SEM/EDX analyses on the worn surface of the GT, PT, and GPT tools after 150-s cutting at the speed of 120 m/min under the dry cutting. Obviously, severe adhesive wear can be seen at the rake face of the GT tools (Fig. 8a), whereas the crater wear can barely be spotted. The corresponding SEM/EDX map of the distribution of Fe elements at the rake face (Fig. 8b) revealed that large number of Fe elements adhered to the area closing to cutting edge and micro-groove area. As is well known, the existence of Fe elements in the rake face is an indication that the workpiece sticks to the tool-chip interface resulting from the adhesive wear mechanism. According to the analysis above, we can conclude that the surface damage was primarily in the form of adhesive wear. We know that under high temperature and high pressure, lubricant can easily be squeezed and ingress into the tool-chip face and then form solid lubricating film between the tool and chip. We know that the lubricant used contain the S elements, while the used tools and workpiece contain no S elements prior to machining. Thus, the existence of S elements can prove the existence of lubricant MoS_2, whereas the corresponding SEM/EDX map of the distribution of the S elements at the rake face (Fig. 8c) illustrated that only a few S elements adhered to the tool-chip interface. It led us to the conclusion that the solid lubricating film at the tool-chip interface was thin and incomplete.

Figure 9 revealed that the crater wear at the rake face of the PT tool was also nearly not observed and much milder adhesive wear compared with the GT tools (see Fig. 8a) under conditions of solid lubricating MoS_2. The corresponding SEM/EDX maps of the distribution of Fe elements (Fig. 9b) can also prove the milder adhesive wear. The corresponding SEM/EDX map of the distribution of S elements (Fig. 9c) at the rake face of PT tool informed us that the solid lubricating film was relatively thicker and more complete compared with GT tools.

Figure 10 indicated that the crater wear at the rake face of GPT tool was not found and mildest adhesive wear among GT tool, PT tool, and GPT tool (see Fig. 10a) under dry cutting, which may be attributed to the hybrid of micro-groove and micro-pit. Another powerful evidence can be the corresponding SEM/EDX maps of the distribution of Fe elements (Fig. 10b). The decreased Fe elements noted that a hybrid-textured structure was likely to exhibit better capability to capture debris that was easy to adhere to the tool-chip contact surface. According to the corresponding SEM/EDX maps of the distribution of S elements (Fig. 10c) at the rake face of GPT tool, we can concluded that the solid lubricating film was thickest and most complete among GT tool, PT tool, and GPT tool. This meant that a hybrid texture was responsible for the promoting lubricant effect.

Apparently, large amount of lubricant trapped in the micro-textures between the tool and workpiece had been squeezed into the tool-chip interface of GPT tools and smeared on the rake face (Fig. 10c), while only a small amount of lubricant could be squeezed onto the tool-chip interface of GT tools and

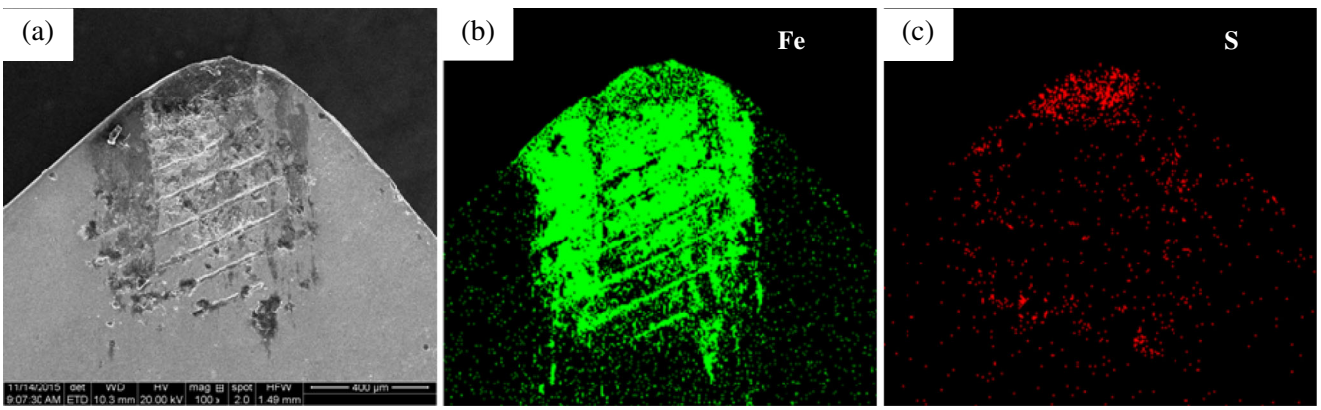

Fig. 8 Micro-graphs of the wear track at the rake face (**a**) and EDX maps of the distribution of Fe and S elements on the worn surface (**b**, **c**) of the GT tool after 150-s cutting at the speed of 120 m/min

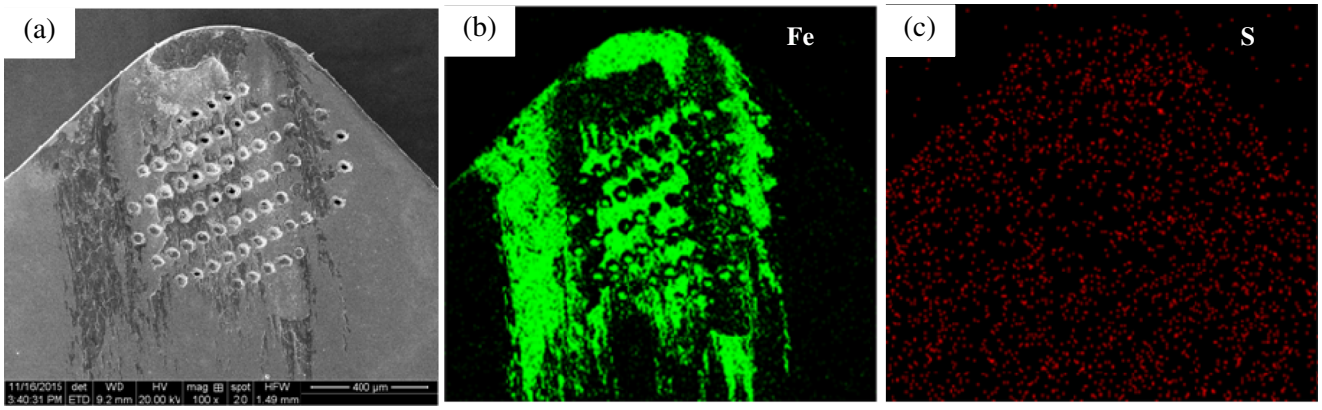

Fig. 9 Micro-graphs of the wear track at the rake face (**a**) and EDX maps of the distribution of Fe and S elements on the worn surface (**b**, **c**) of the PT tool after 150-s cutting at the speed of 120 m/min

PT tools (Figs. 8c and 9c). It can be explained that for CT tools, the rake face is smooth and flat and the tool-chip interface is tight solid contact during turning process; thus, the lubricant could be greatly hard to permeate into the tool-chip interface of CT tools even under full-lubrication condition. However, for micro-textured tools under the condition of solid lubrication, the lubricant can easily be squeezed out or spread over by the rubbing action of the chip flowing over the micro-textures containing solid lubricant to form a lubricating film at the tool-chip interface as shown in Fig. 11. What is more, compared to micro-pits and micro-grooves, the solid lubrication film shaped by hybrid textures of micro-pits and micro-grooves is thicker and more complete, as shown in Fig 11b. A thicker solid lubricant film at the tool-chip interface can further reduce tool-chip friction coefficient and improve tribological property.

As is well known, the motion of lubricant results from the shear force and squeezing force from chip, so inside the lubricating film, the lubricant movement speed decreases along the direction of *Y* axis and basically remains unchanged along the direction of *X* axis. In terms of single texture, the movement of lubricant is stable, whereas for hybrid texture, due to the constantly changing surface texture, fluctuation appears during the motion resulting in a higher speed along the direction of *Y* axis as shown in Fig. 11c. A higher lubricant speed will contribute to forming a thicker lubricating film beyond all doubt. Furthermore, the changing flowing lubricant would produce a larger impact resulting in a higher thrust force. Furthermore, hybrid texture combining multi-arcs and triangle texture may perform a lubricating film with more appropriate pressure distribution and thus produces a higher thrust force.

Under the same squeezing force, the lubricant inside the pit providing relatively airtight compressed volume is prone to move out the pits, whereas the lubricant inside the groove featuring connectivity is prone to move along the groove until the end of the groove and then out the groove. So, it takes shorter time to form solid lubricating film between the tool-chip interface for micro-pitted tool than micro-grooved tool. As we can know from Fig 1, the micro-pits' walls are more abrupt than that of micro-groove. Under the same shear force, the lubricant inside the micro-pit is more likely to move up and down along the walls. Therefore, when the shear force and squeezing force are constant, as the cutting process continues, the pressure around the pit is more prone to increase than that around the groove. Meanwhile, the theory that the micro-pitted surface can effectively improve the surface lubricating

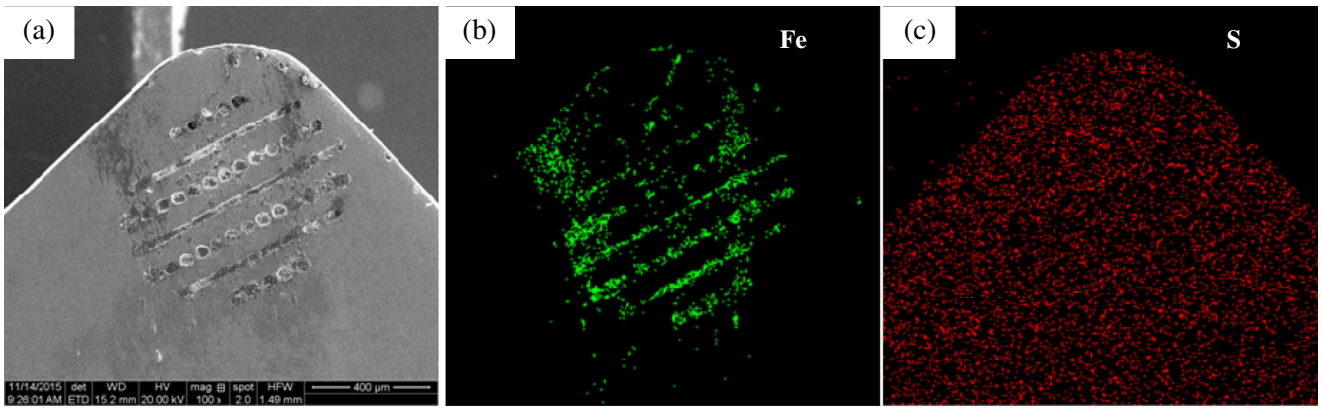

Fig. 10 Micro-graphs of the wear track at the rake face (**a**) and EDX maps of the distribution of Fe and S elements on the worn surface (**b**, **c**) of the GPT tool after 150-s cutting at the speed of 120 m/min

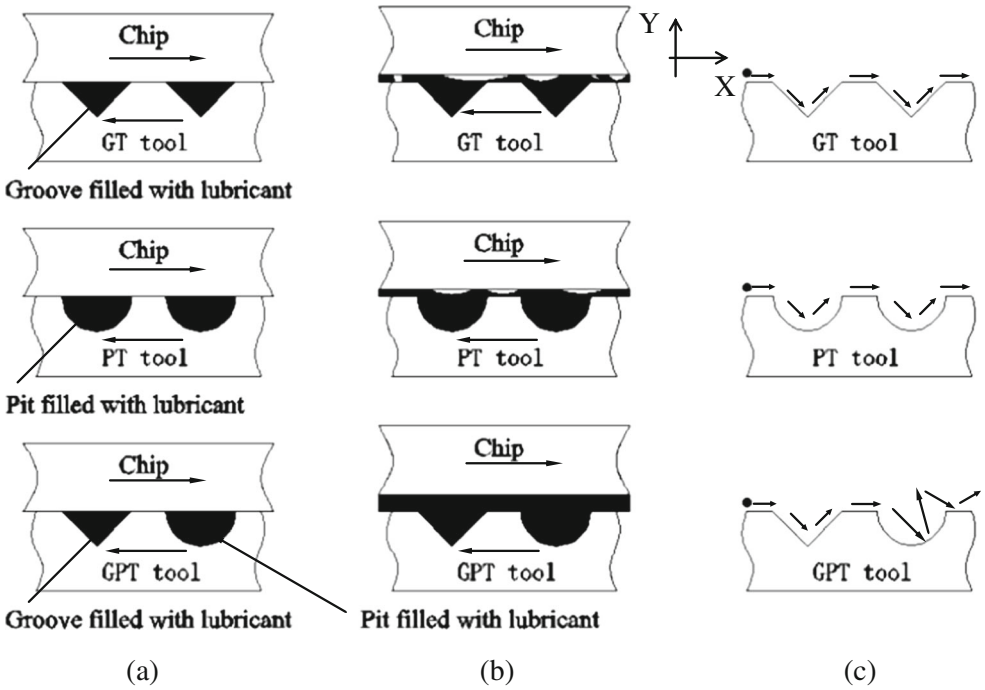

Fig. 11 Lubrication schematic diagram of three different kinds of micro-textured self-lubricating tools, **a** before cutting, **b** lubricating film formed, and **c** the motion of one particle

and thrust forces is explained in friction and cutting experiments [28–30].

The effective bearing area extends by collaborative complementation to increase lubricating film pressure. Yin et al. [21] has confirmed that the high-pressure lubricating film area around micro-pits and the high-pressure lubricating film area beside micro-grooves can implement an effect of enrichment, further increasing the pressure of lubricating film. All this strengthen the ability of lubricating film to resist extrusion and produce a higher thrust force, and then decrease the contact of micro-bulge, reducing the friction. Hence, the cutting forces, average friction coefficient, and tool wear were decreased more effectively. Ruan and Lu [20] suggested that multi-textured surface structured by multi-arcs and triangle texture performed better hydrodynamic in comparison with the independent-textured surface.

Also, the motion of lubricant also results from the squeezing force. Figure 12 illustrates the motion of lubricant resulting from squeezing force. As shown in Fig. 12a, in terms of GT tool, because micro-groove features connectivity, the lubricant inside the groove will flow along the groove to the terminal of the groove due to squeezing. As a result, large amount of lubricant distributes in the area near the cutting edge, while only little distributes in the area between two adjacent grooves. So, the lubricant cannot distribute in the whole tool-chip interface. As demonstrated in Fig. 12b, as far as PT tool is concerned, micro-pit featuring relatively closed nature, the lubricant inside the pit will flow along the upper edge of the pit to the area near the pit. But, the lubricants distributing around the area closing to the cutting edge are only provided by the few pits near the cutting edge. As illustrated in Fig. 12c, for GPT tool, featuring connectivity, micro-

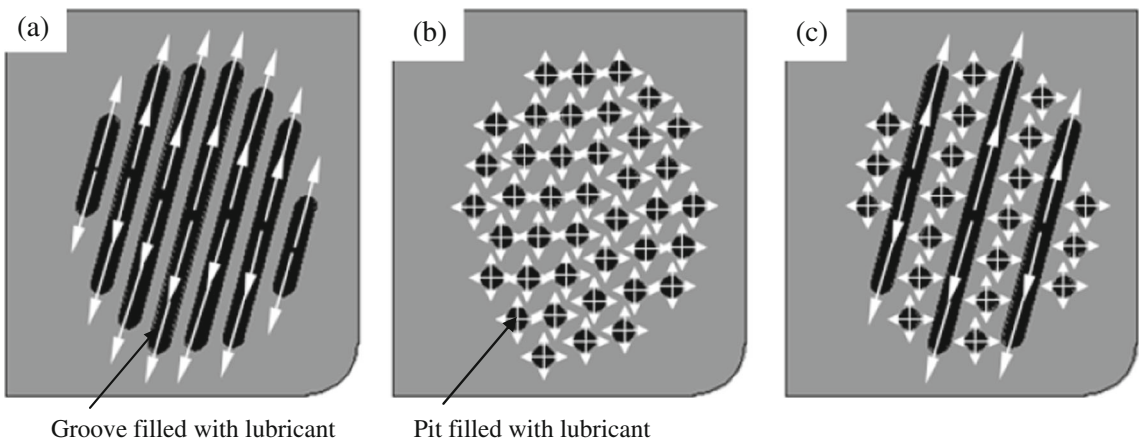

Fig. 12 The lubricant motion due to squeezing, **a** GT tool, **b** PT tool, and **c** GPT tool

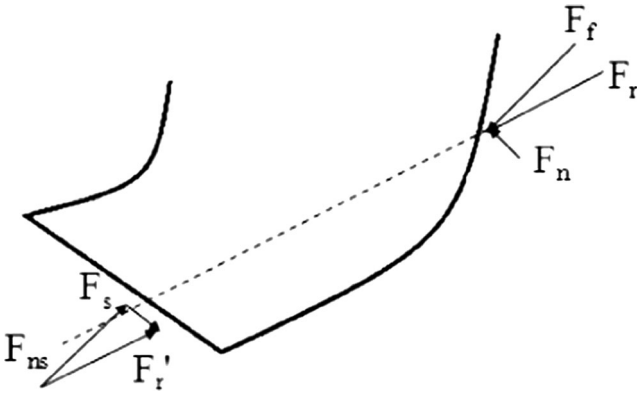

Fig. 13 Moment force model of chip

groove can transfer the lubricant to the area away from the micro-textured area. The lubricant inside the pit distributes in the micro-textured area. In addition, the lubricants inside the pit may enter into the groove and were transferred to the area near the cutting edge. In other words, micro-pit acts the role of reservoir of lubricant, whereas micro-groove plays a part of transport pipeline. Consequently, the lubricant can easily and rapidly distribute in the whole tool-chip interface.

According to image-plasticity method [31], the reason for chip curl is the existence of flexural moment in the cutting process. As shown in Fig. 13, cutting resultant force (F_r) of rake face and cutting thrust force (F_r') are equal and opposite, whereas they are not collinear, which causes the existence of flexural moment. This flexural moment contributes to chip curling and chip breaking.

Based on the viewpoint that flexural moments of a same direction can give rise to the curl in same direction, due to the flexural moment caused by friction in the opposite direction to chip curling, the reduction of friction can contribute to chip curling. It is spontaneous to believe that the curled chip geometry may be related to the friction force reduction due to micro-pool lubrication. The chip curl degree can be used as an estimate for the frictional condition at the tool-chip interface [32, 33]. Figure 14 shows the macro-morphology of chips with CT tool, GT tool, PT tool, and GPT tool with the following parameters: cutting speed $v = 120$ m/min, depth of cut $a_p = 0.2$ mm, and feed rate $f = 0.1$ mm/rev. When used with carbide cutting tools for pure iron during cutting, the chip was composed of two parts, as shown in Fig. 14. One thick layer was called main chip, and the thin layer was named deputy chip. The deputy chip resulted from the violent friction between tool rake face and workpiece [34]. Therefore, an improved tool-chip contact environment can decrease the deputy chip length. So, the length of deputy chip can be another evaluation of the friction environment. Obviously, the chip with CT tool was long and straight, while those with micro-textured self-lubricating tools were short and curled. What is more, the chip with GPT tool was much shorter and more crisp compared with GT and PT tools. It was also found from Fig. 14 that there was almost no deputy chip forming with

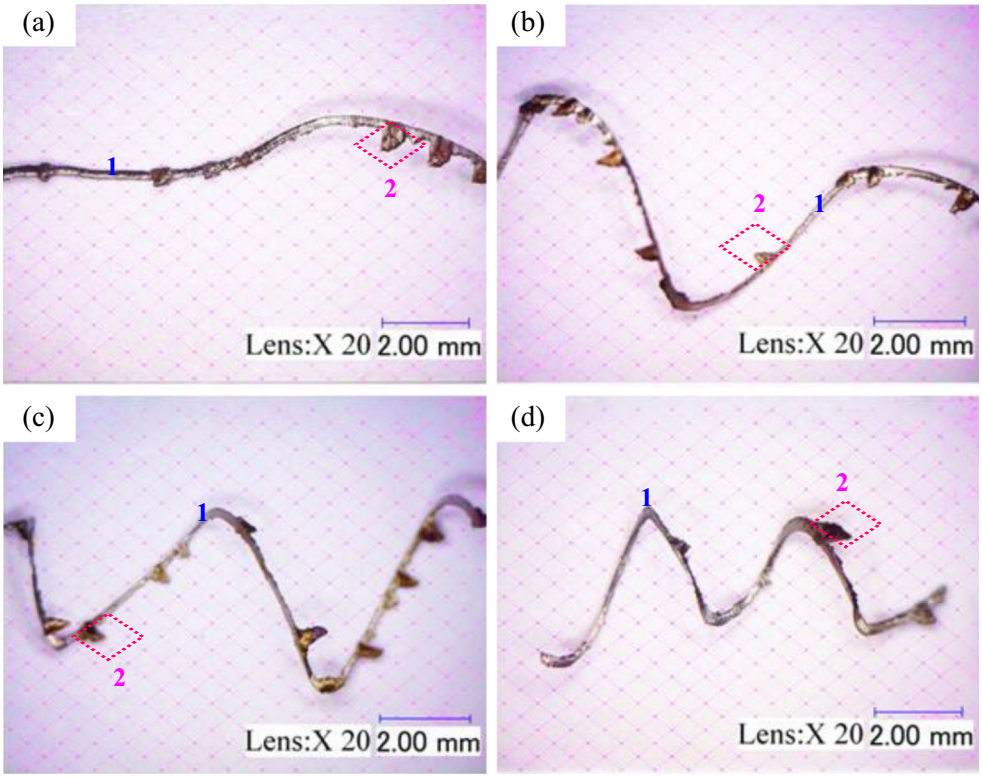

Fig. 14 The macro-morphology of chips with CT tool, GT tool, PT tool, and GPT tool

GPT tool. This is, hybrid texture further improved the tool-chip tribological environment significantly compared to single texture.

The domestic and foreign studies on surface texture improving the tool cutting performance have already gained fruitful achievements but lack systematization and comprehensiveness. However, there are still some aspects needed to further study. The morphology of surface texture is single; literature information referring to hybrid texture are less. Few further studies about complex pattern of surface texture have been conducted, especially the study on the texture patter with variable sizes and densities. The micro-texture is mainly created on the rake face. There are few researches on fabricating texture on the flank face of tool. There are some studies on the wear mechanism; however, they are mainly conducted from qualitative and theoretical analyses, lacking quantization studies [35].

4 Conclusion

In this paper, surface hybrid textures were fabricated on the rake face of the cemented carbide (WC/Co) inserts using laser; then, solid lubricant MoS_2 was embedded into the micro-textures. The hybrid-textured self-lubricating tools were successfully prepared. Cutting tests on pure iron were performed with these developed tools and conventional micro-textured tools under dry cutting conditions, respectively.

The presence of hybrid textures combining micro-pits and micro-grooves by laser technique on rake face brought about the decrease in the cutting forces, cutting temperature, friction coefficient, and tool wear comparing to the single-textured tools. The beneficial hybrid texture effect was evident in the case of high cutting speed (120 m/min), when the cutting forces were reduced by 7.1–33.3 %, the cutting temperature was reduced by 6.9–21.7 %, and the surface roughness R_a was reduced by 42.9–69.1 %.

The beneficial influence of hybrid textures was primarily by the collaborative complementation as micro-reservoir for constant lubricant replenishment of micro-grooves and micro-pits. The hybrid texture contributes to forming a more complete lubricating film at the tool-chip interface in comparison with single texture.

Acknowledgments This work is supported by the Natural Science Foundation of Shandong Province of China (ZR2015EM039) and the Fundamental Research Funds of Shandong Province (2014JC039).

References

1. Shaw MC (2005) Metal cutting principles. New York, USA
2. Xu DM, Huang M, Xia ZH (2011) Study on the cutting performance of ceramic cutting tool in turning pure iron. Mod Manuf Eng 05:85–88
3. Xu DM, Chen H, Kong JX (2014) Study on application of lubrication technology in turning pure iron. Mater Sci Forum 770:116–119
4. Etsion I, Burstein L (1996) A model for mechanical seals with regular micro-surface structure. Tribol Trans 39(3):677–683
5. Etsion I (2004) Improving tribological performance of mechanical components by laser surface texturing. Tribol Lett 17(4):733–737
6. Obikawa T, Kamio A, Takaoka H, Osada A (2011) Micro-texture at the coated tool face for high performance cutting. Int J Mach Tools Manuf 51(12):966–972
7. Sugihara T, Enomoto T (2009) Development of a cutting tool with nano/micro-textured surface: improvement of anti-adhesive effect by considering the texture patterns. Precis Eng 33(4):425–429
8. Qian S, Zhu D, Qu N, Li H, Yan DS (2010) Generating micro-dimples array on the hard chrome-coated surface by modified through mask electrochemical micromachining. Int J Adv Manuf Technol 47(9–12):1121–1127
9. Shen XH, Tao GC (2015) Tribological behaviors of two micro textured surfaces generated by vibrating milling under boundary lubricated sliding. Int J Adv Manuf Technol: 1–8
10. Sugihara T, Enomoto T (2012) Improving anti-adhesion in aluminum alloy cutting by micro stripe texture. Precis Eng 36(2):229–237
11. Evans CJ, Bryan JB (1999) "Structured" "textured" or "engineered" surfaces. CIRP Ann Manuf Technol 48(2):541–556
12. Machado AR, Wallbank J (1994) The effects of a high-pressure coolant jet on machining. Proc Inst Mech Eng B J Eng Manuf 208(1):29–38
13. Hong SY, Ding Y, Jeong J (2002) Experimental evaluation of friction coefficient and liquid nitrogen lubrication effect in cryogenic machining. Mach Sci Technol 6(2):235–250
14. Dumitru G, Romano V, Gerbig Y, Weber HP, Haefke H (2005) Femtosecond laser processing of nitride-based thin films to improve their tribological performance. Appl Phys A 80(2):283–287
15. Wei W, Lankford J, Kossowsky R (1987) Friction and wear of ion-beam-modified ceramics for use in high temperature adiabatic engines. Mater Sci Eng 90:307–315
16. Julthongpiput D, Ahn HS, Sidorenko A, Kim DI, Tsukruk VV (2002) Towards self-lubricated nanocoatings. Tribol Int 35(12): 829–836
17. Deng JX, Ding ZL, Zhao J, Wang JH, Ai X (2003) Development of the high-temperature self-lubricating ceramic tool materials and its cutting performance. Chin J Mech Eng 39(8):106–109
18. Deng JX, Ge PQ, Ai X (2003) Development and perspective of lubricating techniques in metal cutting. Tribology 23:546–550
19. Segu DZ, Choi SG, Hyouk Choi J, Kim SS (2013) The effect of multi-scale laser textured surface on lubrication regime. Appl Surf Sci 270:58–63
20. Ruan HY, Lu JJ (2010) Hydrodynamic lubrication performance on multi-textured surface structured by multi-arcs and triangle textures. J Jiangsu Univ (Nat Sci Edn) 3, 003
21. Yin BF, Qian AQ, Lu ZT, Wang BW, Sun A (2014) Theoretical and experimental study on lubrication performance of composite textures on cylinder liners. J Xian Jiaotong Univ 48(9):74–80
22. Chen RY (2000) Metal cutting principles. Beijing, China
23. Tian WS, Le DQ (1990) The study of cutting performance of pure iron. J Taiyuan Heavy Mach Inst 2:002
24. Kong JX, Li L, Xu DM, He N (2014) Study on tool life and tool wear mechanisms in dry cutting pure iron. Mater Sci Forum 770: 74–77
25. Lei ST, Devarajan S, Chang ZH (2009) A comparative study on the machining performance of textured cutting tools with lubrication. Int J Mech Manuf Syst 2(4):401–413
26. Marinov VR (2001) Hybrid analytical–numerical solution for the shear angle in orthogonal metal cutting—part I: theoretical foundation. Int J Mech Sci 43(2):399–414

27. Recht RF (1985) A dynamic analysis of high-speed machining. J Manuf Sci Eng 107(4):309–315
28. Erdemir A (2005) Review of engineered tribological interfaces for improved boundary lubrication. Tribol Int 38(3):249–256
29. Cordier-Robert C, Crampon J, Foct J (1998) Surface alloying of iron by laser melting: microstructure and mechanical properties. Surf Eng 14(5):381–385
30. De Damborenea J (1998) Surface modification of metals by high power lasers. Surf Coat Technol 100:377–382
31. Fu H, Chen YJ (1998) Research on the principle of cutting process of cutters with friction-decreasing grooves. Tool Eng 32(2):7–10
32. Lei ST, Devarajan S, Chang ZH (2009) A study of micro-pool lubricated cutting tool in machining of mild steel. J Mater Process Technol 209(3):1612–1620
33. Kim DM, Bajpai V, Kim BH, Park HW (2015) Finite element modeling of hard turning process via a micro-textured tool. Int J Adv Manuf Technol 78(9–12):1393–1405
34. Wang YH (1996) Alloy cast iron cutting principles. Jiang Su, China
35. Sun JL, Zhou YH, Deng JX (2015) Research on textured coating tool. Tool Eng 7:002